Nâng cao hiệu suất cảm biến khí VOCs của màng mỏng ZnO thông qua biến tính bề mặt bằng hạt nano Au và chiếu bức xạ UV

TÓM TẮT

Các hợp chất hữu cơ dễ bay hơi (VOCs), chẳng hạn như isopropanol (IPA), gây ra những rủi ro đáng kể cho sức khỏe và môi trường, làm nổi bật nhu cầu về các cảm biến khí có độ nhạy cao, chọn lọc và tiết kiệm năng lượng. ZnO là một vật liệu cảm biến đầy hứa hẹn do có dải cấm rộng, độ linh động electron cao và đặc tính hấp phụ khí mạnh. Tuy nhiên, các cảm biến ZnO tinh khiết thường yêu cầu nhiệt độ làm việc cao và thiếu tính chọn lọc. Công trình này nghiên cứu các màng mỏng ZnO được biến tính bằng hạt nano Au để tăng cường nhạy IPA dưới bức xạ UV 365 nm. Các màng ZnO và hạt nano Au được lắng đọng bằng phương pháp phún xạ. Các phân tích về cấu trúc và thành phần được thực hiện bằng kính hiển vi điện tử quét phát xạ trường (FE-SEM), nhiễu xạ tia X (XRD) và phổ tán xạ năng lượng tia X (EDS). Kết quả cho thấy các hạt nano Au hoạt động như các vị trí xúc tác, cải thiện quá trình truyền điện tích và quá trình oxy hóa khí, do đó tăng cường độ nhạy. Các hạt tải quang sinh do tia UV tạo ra giúp tăng hiệu suất của cảm biến. Các màng ZnO được biến tính bởi các hạt nano Au thể hiện khả năng hồi đáp vượt trội, với hiệu suất tối ưu ở mức hàm lượng Au vừa phải. Hoạt động hỗ trợ của tia UV cho phép phát hiện IPA hiệu quả ở nhiệt độ thấp hơn, giảm mức tiêu thụ điện năng. Những phát hiện này góp phần vào việc thiết kế các cảm biến VOCs thế hệ tiếp theo cho các ứng dụng trong môi trường và công nghiệp.

Từ khoá: *Cảm biến khí VOC, ZnO, màng mỏng, isopropanol, hạt nano Au.*

Enhancing VOCs gas sensing performance of ZnO thin films via Au nanoparticles surface modification and UV illumination

ABSTRACT

Volatile organic compounds (VOCs), such as isopropanol (IPA), pose significant health and environmental risks, highlighting the need for highly sensitive, selective, and energy-efficient gas sensors. Zinc oxide (ZnO) is a promising sensing material due to its wide bandgap, high electron mobility, and strong gas adsorption properties. However, pristine ZnO sensors often require high operating temperatures and lack selectivity. This study investigates Au nanoparticle-modified ZnO thin films for enhanced IPA sensing under 365 nm UV illumination. ZnO films were deposited via RF sputtering, with Au nanoparticles added using DC sputtering. Structural and compositional analyses were performed using field-emission scanning electron microscopy (FE-SEM), X-ray diffraction (XRD), and energy-dispersive X-ray spectroscopy (EDS). Results show that Au nanoparticles act as catalytic sites, improving charge transfer and gas oxidation, thereby enhancing sensitivity. UV-generated charge carriers boost sensor performance. Au-decorated ZnO films exhibit superior response characteristic, with optimal performance at moderate Au loading. UV-assisted operation enables efficient gas detection at lower temperatures, reducing power consumption. These findings contribute to the design of next-generation VOC sensors for environmental and industrial applications.

Keywords: *VOCs gas sensing, ZnO, thin film, isopropanol, Au nanoparticles.*

1. INTRODUCTION

Volatile organic compounds (VOCs), such as isopropanol (IPA), are widely used in industrial, medical, and household applications.[1] However, prolonged exposure to IPA vapors can cause serious health risks, including respiratory and neurological issues, as well as environmental harm.[2] Therefore, developing highly sensitive, selective, and energy-efficient gas sensors for IPA detection is essential for air quality monitoring and workplace safety. Among various sensing materials, zinc oxide (ZnO) stands out due to its wide bandgap (~3.37 eV), high electron mobility, and strong adsorption-desorption properties.[3]

Zinc oxide (ZnO) is widely used in gas sensors due to its unique electronic properties and strong interaction with gas molecules.[4,5] Exposure to VOCs causes gas molecules to adsorb and react on the ZnO surface, altering charge carrier concentration and changing electrical conductivity.[6] ZnO nanomaterials, such as nanorods, nanowires, and nanosheets, show enhanced sensing performance due to their high surface-area-to-volume ratio, which promotes gas adsorption.[7] However, pristine ZnO sensors often lack selectivity and require high operating temperatures, necessitating material modifications for improved performance.[8]

ZnO-based gas sensors typically operate at elevated temperatures (200–400 °C) to enhance the adsorption and reaction of gas molecules on the surface. However, high-temperature operation not only increases power consumption but also accelerates material degradation, reducing the sensor's lifetime.[8] To address these limitations, researchers have explored two key strategies to enhance the gas sensing performance of ZnO at lower temperatures: (1) surface modification with noble metal nanoparticles (NPs) and (2) photoactivation using ultraviolet (UV) light.

Noble metal NPs, such as Au, Ag, and Pt, act as catalysts to improve the reaction kinetics of gas molecules, while UV illumination generates additional charge carriers, enhancing the sensor response at room temperature.[9,10] Gold (Au) nanoparticles, in particular, have been extensively studied for their excellent catalytic properties and ability to form Schottky junctions with ZnO, which modulate charge transport and improve sensor selectivity.[11] The catalytic effect of Au facilitates the oxidation of IPA molecules by promoting charge transfer between the gas and the semiconductor surface, leading to a more pronounced change in electrical conductivity.[12] The incorporation of Au NPs onto ZnO surfaces significantly enhances gas sensing performance through multiple mechanisms. Previous studies have demonstrated that Au-modified ZnO sensors exhibit superior performance in detecting VOCs such as ethanol, acetone, and toluene, making Au a promising dopant for IPA sensing applications.[13]

UV irradiation is an effective approach to lower the operating temperature of ZnO gas sensors by generating photogenerated electron-hole pairs that participate in gas sensing reactions.[14] The energy of UV photons excites electrons from the valence band (VB) to the conduction band (CB) of ZnO, increasing charge carrier concentration and enhancing gas adsorption and/or desorption dynamics.[15] Studies have reported that UV-assisted ZnO sensors can operate efficiently at room temperature, making them suitable for low power and portable sensing applications.[16,17]

The combination of Au NPs and UV illumination in ZnO-based gas sensors has shown a synergistic enhancement in sensing performance. The catalytic activity of Au NPs accelerates gas oxidation, while UV-induced charge carrier generation further amplifies the sensor response.[18] This dual enhancement mechanism enables the detection of VOCs with higher sensitivity, lower detection limits, and improved response/recovery times. Recent studies have demonstrated that Au-ZnO hybrid sensors exhibit remarkable performance in detecting ethanol, formaldehyde, and acetone, but limited research has focused on IPA detection.[19]

In this study, we focus on the fabrication and characterization of ZnO thin films modified with Au nanoparticles for IPA sensing under 365 nm UV irradiation. The choice of ZnO thin films, rather than nanostructured ZnO powders, is motivated by their superior stability, uniformity, and compatibility with integrated sensor devices.[20,21] By combining the catalytic activity of Au nanoparticles with the photoactivation effect of UV light, we aim to achieve enhanced sensitivity, lower detection limits, and reduced operating temperature for IPA detection. The findings of this study will provide valuable insights into the design of next-generation gas sensors for VOCs monitoring in environmental and industrial applications.

2. EXPERIMENTAL

Substrates integrated with Au electrodes (5 mm × 5 mm × 0.1 mm) underwent sequential ultrasonic cleaning in acetone, methanol, and deionized water for 15 minutes each, followed by nitrogen blow-drying. Subsequently, thin ZnO films were deposited onto the pre-patterned substrates via radio frequency (RF) sputtering of a high-purity (99.99%) ZnO target using a shadow mask. The deposition process was conducted at room temperature under an Ar pressure of 10 mTorr, with an input power of 50 W. To enhance structural integrity, the ZnO-coated substrates were thermally oxidized in ambient air at 400 °C for 1 hour, with a heating rate of 12.5 °C/min. During oxidation, the ZnO films underwent morphological evolution, exhibiting agglomeration into dome-like nanoparticles rather than maintaining planar surfaces.

The ZnO film substrates were further functionalized with Au nanoparticles via direct current (DC) sputtering of an Au target under identical deposition conditions: room temperature, 10 mTorr Ar pressure, and 50 W input power. The thicknesses of both the ZnO and Au layers were meticulously monitored using a quartz crystal microbalance sensor to ensure deposition precision. To promote structural stability and optimize surface dispersion, the samples were subjected to post-deposition annealing at 400 °C for 1 hour in ambient air, with a heating rate of 25 °C/min. It is expected that this process facilitated the uniform distribution of Au nanoparticles across the ZnO film surface.

To distinguish the samples, the ZnO films were labeled as ZnO25, ZnO50, ZnO100, and ZnO150, corresponding to their nominal thicknesses (monitored by the quartz microbalance sensor) of 25 nm, 50 nm, 100 nm, and 150 nm, respectively. After Au sputtering, the samples were further named based on the Au layer thickness, such as ZnO25/Au2.5, ZnO50/Au5, ZnO100/Au10, and ZnO150/Au15 for Au thicknesses of 2.5 nm, 5 nm, 10 nm, and 15 nm. However, cross-sectional SEM measurements indicated significant deviations from the intended thicknesses.

The surface morphology and structural characteristics of the sensing film were systematically analyzed using field-emission scanning electron microscopy (FE-SEM; HITACHI S-4800), X-ray diffraction (XRD; Bruker D2, equipped with Cu Kα, $\lambda = 1.5406$ Å radiation) and energy-dispersive X-ray spectroscopy (EDS). The experimental setup for gas sensing measurements is schematically depicted in previous works.[22,23] The sensing performance was evaluated using a high-precision micro-ammeter/voltage source (Keithley 2601B). VOCs, generated through a bubble evaporator with an air carrier gas, served as the target analytes. The VOCs concentration was precisely regulated by diluting the vapor with dry air at a constant flow rate of 500 sccm before its introduction into the test chamber.

3. RESULTS AND DISCUSSION

3.1. Morphology, structure, and chemical composition of the sensing film

The FE-SEM images provide significant insights into the morphological properties of the ZnO and Au-decorated ZnO thin films. For the pure ZnO films (Figure 1), the FE-SEM images indicate the formation of ZnO nanoparticles, which agglomerate into dome-shaped particles during the oxidation process. The size of these nanoparticles increases with the initial thickness of the deposited film. This agglomeration is due to high-temperature annealing, which promotes grain growth and the coalescence of smaller particles. While the distribution of nanoparticles is relatively uniform, certain regions exhibit denser clustering, potentially affecting the film's overall homogeneity and surface area. Furthermore, the measured thicknesses of 160 nm for ZnO100 and 250 nm for ZnO150 (as shown in the insets of Figure 1) significantly deviate from their nominal values of 100 nm and 150 nm, respectively. This discrepancy suggests variations in the sputtering process, such as differences in deposition rates or post-deposition oxidation effects. The non-uniform thickness may impact the electrical and sensing properties of the films, underscoring the importance of precise control over deposition parameters.

In the case of Au-decorated ZnO films (Figure 2), the FE-SEM images demonstrate the successful deposition of Au nanoparticles on the ZnO surface. For ZnO100/Au5, the Au nanoparticles are uniformly distributed with smaller sizes, while ZnO100/Au10 exhibits larger and more densely packed Au clusters. The increased Au thickness enhances the surface coverage, which could improve the catalytic activity and gas adsorption capabilities of the material. However, excessive clustering of Au nanoparticles might reduce the effective surface area, potentially impacting the sensor's performance. The presence of ZnO nanoparticles

beneath the Au layer provides a high surface area substrate, which is beneficial for gas sensing applications. The interaction between the Au nanoparticles and the ZnO surface is crucial, as it can enhance the charge transfer processes and improve the sensitivity towards volatile organic compounds (VOCs). These findings underscore the importance of optimizing both the ZnO nanoparticle formation and Au thickness and distribution to achieve enhanced gas sensing properties.

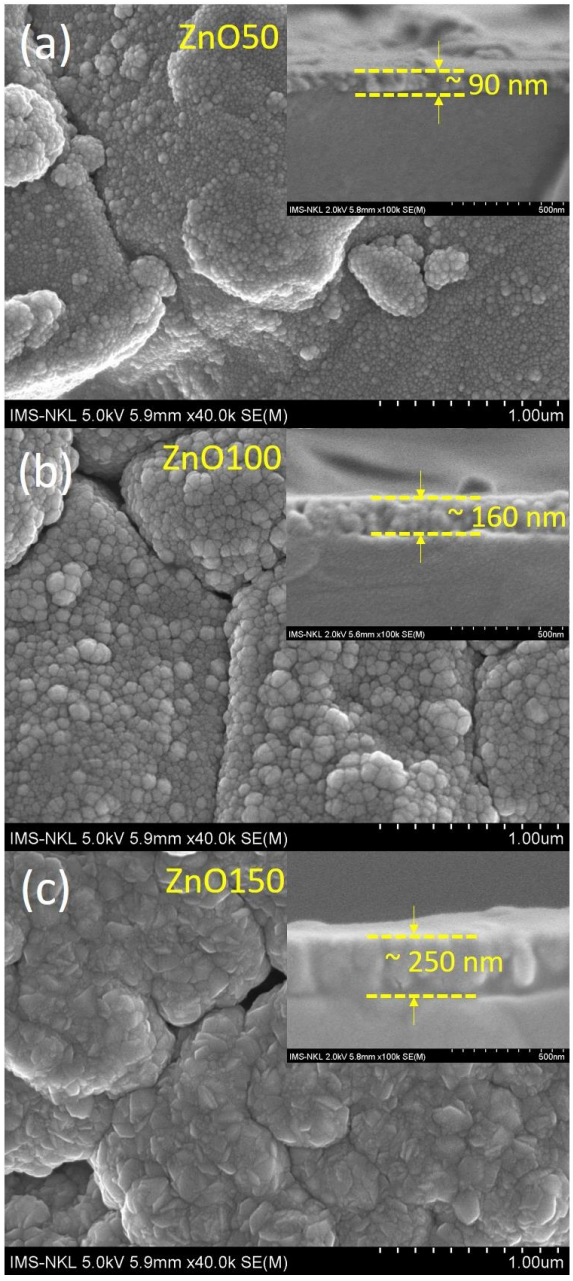

Figure 1. Surface FE-SEM images of pure ZnO thin films: (a) ZnO50, (b) ZnO100, and (c) ZnO150. Insets show corresponding cross-sectional views.

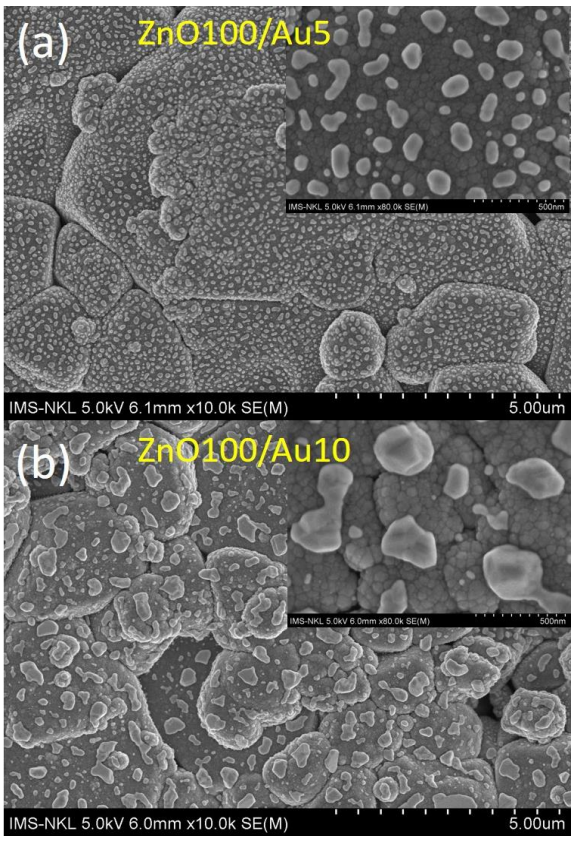

Figure 2. Surface FE-SEM images of Au-decorated ZnO thin films: (a) ZnO100/Au5 and (b) ZnO100/Au10. The insets show corresponding higher-magnification views.

The EDS spectra presented in Figure 3 confirm the elemental composition of the ZnO100/Au2.5, ZnO100/Au5, ZnO100/Au10, and ZnO100/Au15 samples. The spectra exhibit characteristic peaks corresponding to Zn (zinc), O (oxygen), and Au (gold), which validate the successful deposition of gold onto the ZnO surface. The intensity of the Au peaks increases progressively with the nominal thickness of the sputtered gold layer, indicating a systematic augmentation in gold content. Additionally, a minor Al (aluminum) signal is detected, which originates from the substrate.

The inset graph in Figure 3 quantitatively illustrates the atomic percentage of Au in relation to the nominal thickness of the deposited layer. A clear positive correlation is observed, with the Au content increasing as the nominal thickness rises from 2.5 nm to 15 nm. The error bars, which remain relatively small, indicate a high degree of measurement accuracy and reproducibility. The consistency between the EDS spectra and the atomic percentage data further corroborates the uniform deposition of gold.

Overall, these findings confirm the controlled growth of Au layers on ZnO films, with

elemental compositions aligning well with the expected deposition parameters. The presence of Zn and O peaks further verifies the integrity of the underlying ZnO layer. The data not only substantiate the effectiveness of the sputtering process but also establish a foundation for subsequent investigations into the physicochemical properties of these nanostructured materials.

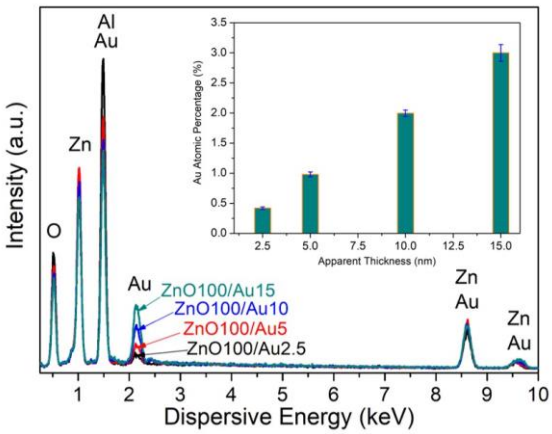

Figure 3. EDS spectra of the ZnO100/Au2.5, ZnO100/Au5, ZnO100/Au10, and ZnO100/Au15 samples. The inset shows the atomic percentage of Au element in the samples versus the nominal thickness.

Figure 4(a) presents the XRD patterns of ZnO thin films with varying thicknesses (ZnO25, ZnO50, ZnO100, and ZnO150), revealing the characteristic diffraction peaks of hexagonal wurtzite ZnO. The predominant peaks observed at $2\theta \approx 31.8°$, 34.4°, and 36.6° correspond to the (100), (002), and (101) crystal planes, respectively, in accordance with the JCPDS card No. 36-1451. Notably, as the film thickness increases, the intensity of these peaks strengthens, indicating an enhancement in crystallinity. The presence of a minor peak near $2\theta \approx 43.5°$ is attributed to the sample holder rather than the film itself.

Figure 4(b) illustrates the XRD spectra of ZnO100 before and after gold deposition with varying nominal thicknesses (1 nm, 2.5 nm, 5 nm, 10 nm, and 15 nm). The ZnO diffraction peaks remain unchanged, suggesting that the deposition of Au does not significantly alter the ZnO crystal structure. However, the emergence of additional peaks at $2\theta \approx 38.2°$ and 44.4°, corresponding to the (111) and (200) planes of face-centered cubic (FCC) Au (JCPDS No. 04-0784), confirms the successful incorporation of gold onto the ZnO surface. The intensity of the Au(111) peak increases progressively with greater Au thickness, indicating a higher surface coverage and possible nanoparticle growth. Importantly, the absence of any noticeable shift in ZnO peak positions suggests that Au primarily forms a surface layer rather than diffusing into the ZnO lattice. These results validate the controlled deposition of Au on ZnO thin films, preserving the intrinsic wurtzite structure of ZnO while introducing a well-defined Au phase. This structural integrity is crucial for subsequent investigations into the functional properties of these Au-ZnO hybrid materials, particularly in applications.

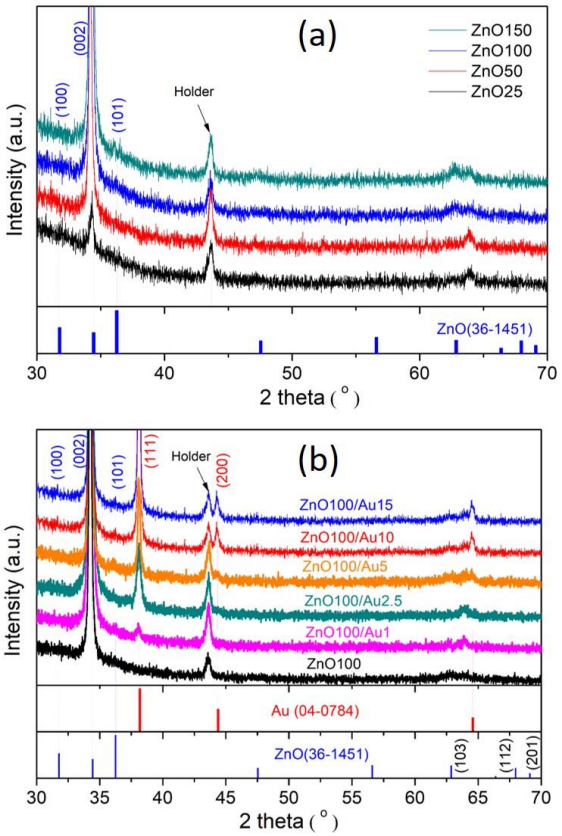

Figure 4. XRD patterns of (a) ZnO films with varying thicknesses and (b) ZnO100 film before and after Au deposition at different thicknesses. Reference patterns for ZnO (JCPDS No. 36-1451) and Au (JCPDS No. 04-0784) are shown for comparison.

3.2. VOCs sensing performance

The bar chart (Figure 5) shows the ZnO100 sensor's response to various gases at 1000 ppm and 250°C under dark conditions. The response of the sensor was defined by the R_a/R_g ratio, where R_a is the baseline resistance of the sensor in dry air and R_g is the resistance upon exposure to VOCs vapor at a given temperature. In this study, target gases were generated using a bubble evaporator system, in which dry air was passed through a glass bubbler containing the

liquid analyte at room temperature. The saturated vapor was then mixed with a controlled flow of dry air using calibrated mass flow controllers to obtain the desired gas mixture. Based on the physical properties of the analytes (vapor pressure and density), the concentrations of the generated gases were calculated as follows: Toluene: 0.285% (2850 ppm), Acetone: 2.37% (23,700 ppm), Ethanol: 0.583% (5830 ppm), Methanol: 1.275% (12,750 ppm), Isopropanol (IPA): 0.635% (6350 ppm), CO_2: 4% (40,000 ppm), CH_4: 4% (40,000 ppm). These gas concentrations were used in the actual sensing tests. For comparative purposes, the response values were normalized to a reference concentration of 1000 ppm by assuming a near-linear response in the low-concentration range. This normalization allows for clearer discussion of the sensor's selectivity and sensitivity toward different analytes, independent of their initially tested concentrations.

The sensor responds most strongly to toluene, followed by IPA and ethanol, with moderate sensitivity to acetone and methanol. In contrast, CO_2 and CH_4 elicit negligible responses, indicating poor response to non-reactive gases. The inset graph in Figure 5 reveals the sensor's dynamic response to toluene, demonstrating excellent repeatability and stability across multiple cycles. The fabricated sensors exhibited n-type behavior of the semiconductor because of decreasing resistance of the sensor upon exposure to the reducing VOCs vapor. These results highlight the sensor's effectiveness in detecting aromatic and oxygenated VOCs, particularly toluene and IPA, while showing selectivity against non-polar gases. This ZnO-based sensor holds promise for applications in air quality monitoring and VOC detection.

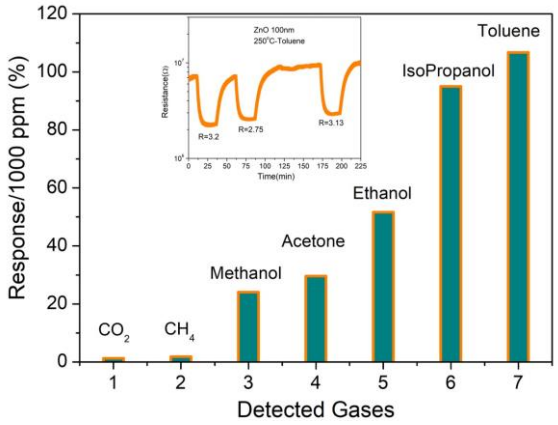

Figure 5. Response of the ZnO100 sensor to various VOCs vapors at 250°C (relative to 1000 ppm). Inset shows resistance response to 2854.8 ppm toluene vapor over three measurement cycles at 250°C.

The gas sensing performance of the ZnO100 sensor toward toluene is significantly influenced by both operating temperature and UV 365 nm irradiation, as illustrated in Figure 6(a). In the absence of UV illumination, the sensor's response gradually increases with temperature. However, under UV 365 nm irradiation, the sensor exhibits an enhanced response even at lower temperatures, demonstrating more stable and consistent behavior. Notably, at 200 °C, the sensor under UV irradiation achieves a response comparable to that observed at higher temperatures in the dark, underscoring the role of UV illumination in activating surface reactions and improving sensitivity.

The inset graph in Figure 6(a) provides further insight into the sensor's dynamic behavior at 200 °C. Without UV illumination, the sensor exhibits a high baseline resistance and incomplete recovery, as the resistance fails to return to its initial state after toluene exposure. This incomplete recovery suggests strong molecular adsorption on the ZnO surface, with insufficient thermal energy at 200 °C to facilitate desorption. Consequently, the sensor experiences signal drift and performance degradation over time. In contrast, under UV 365 nm irradiation, the sensor demonstrates significantly improved recovery, with the resistance fully returning to its initial state after each exposure cycle. This behavior indicates that UV illumination enhances the desorption of adsorbed toluene molecules, due to the generation of photogenerated charge carriers that accelerate surface reactions. The increased electron-hole pairs promote the oxidation of hydrocarbons, effectively resetting the sensor to its baseline state. Additionally, the response magnitude ($R \approx 2.65$) is notably higher under UV illumination compared to the dark condition, further highlighting the role of UV light in enhancing the sensor's sensitivity and stability. These findings emphasize the critical role of UV 365 nm irradiation in improving the ZnO sensor's gas sensing performance, reversibility, and operational efficiency at moderate temperatures. The combination of UV activation and optimized working temperature enables reliable and real-time detection of toluene, making this approach highly beneficial for practical gas sensing applications.

Interestingly, as shown in Figure 6(a), the response of the ZnO sensor at 225 °C under dark conditions was observed to be higher than that under UV 365 nm illumination. This counterintuitive result can be attributed to the

thermal dominance at elevated temperatures, where thermally activated surface reactions are already highly efficient, rendering the additional contribution from UV-generated electron–hole pairs less significant. Moreover, UV irradiation may induce desorption of adsorbed oxygen species or VOC molecules, thereby reducing the density of reactive species on the surface. Additionally, UV light at high temperature could alter the reaction dynamics, possibly forming intermediate species that do not significantly contribute to charge transfer. These combined effects may lead to a decrease in sensing response under UV illumination at higher operating temperatures.

Figure 6(b) shows the response of ZnO sensors with different thicknesses (25–150 nm) to toluene at 200 °C under UV 365 nm irradiation. The response increases with thickness up to 100 nm, after which it decreases for the 150 nm sample. This non-monotonic trend can be attributed to the interplay between surface area and charge transport characteristics: (1) For thin films (ZnO25 and ZnO50 have thicknesses smaller than 90 nm, as estimated by FE-SEM (see Figure 1)), the limited active surface area results in lower gas molecule adsorption and, consequently, a weaker response; (2) For the optimal thickness (ZnO100 has a thickness of approximately 160 nm, as estimated by FE-SEM (see Figure 1)), a balance is achieved between surface reaction sites and efficient charge transport, leading to the highest response; (3) For thicker films (ZnO150 has a thickness of approximately 250 nm, as estimated by FE-SEM (see Figure 1)), the increased bulk volume promotes higher charge carrier recombination and reduced surface activity, thereby diminishing sensing performance. A 100 nm ZnO thickness is identified as the optimal condition under UV irradiation at 200 °C, striking a balance between surface reactivity and charge transport efficiency.

The sensing performance of metal oxide semiconductors depends critically on the interplay between surface reaction activity and charge transport efficiency. An optimal sensing layer morphology allows a balance between a sufficient number of active surface sites for gas adsorption and efficient transport of charge carriers generated during gas–solid interactions. If the film is too thin, the limited surface area reduces gas adsorption; if it is too thick or overly porous, carrier transport is hindered due to increased scattering and recombination at grain boundaries and defects, ultimately lowering the sensor response. Therefore, a moderate film thickness with a controlled nanostructure enhances the response by maximizing both surface reactivity and carrier mobility.[4]

Moreover, an excessive increase in bulk volume may lead to enhanced charge carrier recombination. As charge carriers generated from surface reactions travel through a thicker matrix, they are more to recombine before reaching the electrode, especially in the presence of crystal defects or poor connectivity. This recombination reduces the effective modulation of electrical resistance and thus the sensing response.[16,17,24,25]

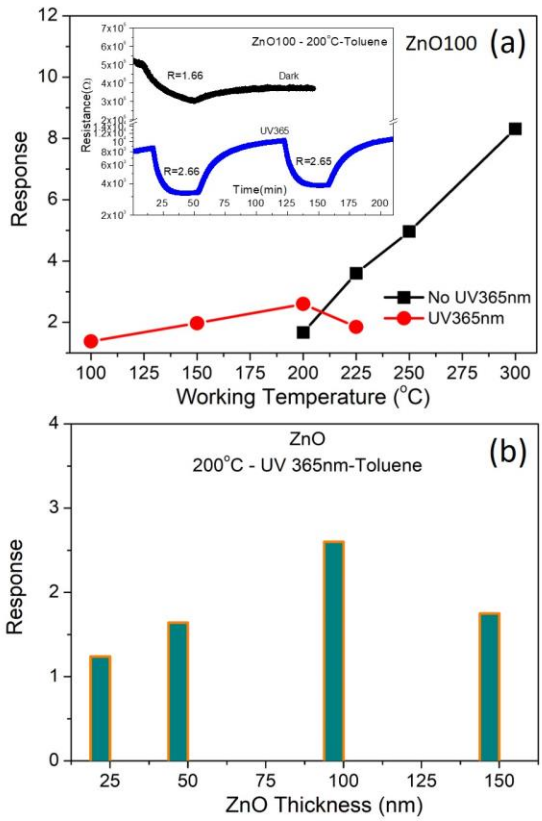

Figure 6. (a) Response of the ZnO100 sensor to 2854.8 ppm toluene vapor as a function of operating temperature under dark conditions (black squares) and UV365nm irradiation (red circles). The inset shows the dynamic resistance of ZnO100 sensor at 200°C in the dark and under UV illumination. (b) Response of ZnO100 sensors with different thicknesses to 2854.8 ppm toluene vapor at the optimized operating temperature of 200°C under UV365nm irradiation.

The sensing performance of the ZnO100/Au10 sensor toward various volatile organic compounds (VOCs) under UV 365 nm irradiation at 200 °C is illustrated in Figures 7(a) and 7(b). In Figure 7(a), the dynamic resistance curves exhibit a distinct decrease upon exposure

to different VOC vapors, followed by a gradual recovery when the detected gas flow is stopped. Notably, the response and recovery characteristics vary significantly depending on the target gas. Among the tested VOCs, IPA induces the most pronounced resistance drop, followed by toluene, ethanol, methanol, and acetone, highlighting the sensor's differential sensitivity. Furthermore, the complete recovery of resistance to its baseline after gas removal demonstrates the excellent reversibility of the ZnO100/Au10 sensor under UV irradiation, a critical feature for practical sensing applications.

Figure 7(b) quantifies the sensor's response, normalized per 1000 ppm of each gas. The results confirm the dynamic response trend observed in Figure 7(a), with IPA exhibiting the highest response, followed by toluene, ethanol, methanol, and acetone. The significantly enhanced response toward IPA and toluene suggests that the ZnO100/Au10 sensor has a strong affinity for these analytes, due to favorable surface interactions and catalytic effects induced by the Au nanoparticles. These findings highlight the sensor's capability for VOC detection with high selectivity, high response, and efficient recovery, making it a promising candidate for real-world gas sensing applications.

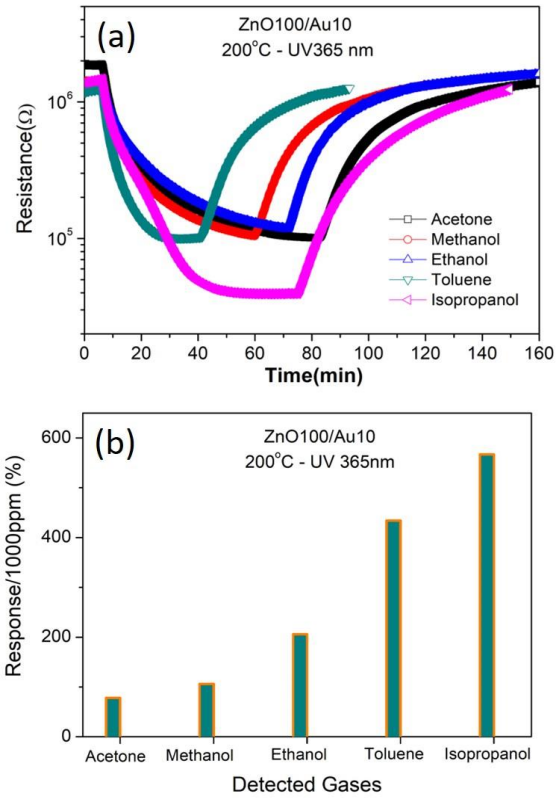

Figure 7. (a) Resistance response of the ZnO100/Au10 sensor to various VOCs and (b) the sensor's response normalized per 1000 ppm of each gas at 200 °C under UV365nm irradiation

The gas sensing characteristics of Au-modified ZnO sensors toward IPA under UV 365 nm irradiation at 200 °C are illustrated in Figures 8(a) and 8(b), emphasizing the impact of Au nanoparticle size and the sensor's response across varying gas concentrations. Figure 8(a) depicts the sensor's response as a function of the Au nominal thickness (which was measured in real-time by the sensor throughout the gold deposition process), revealing that the ZnO100/Au5 sensor achieves the highest response, while thinner (nominal thickness of 2.5 nm) or thicker (The nominal thickness exceeds 10 nm) Au layers significantly diminish performance. This trend suggests that a 5 nm Au layer represents the optimal thickness, striking a balance between catalytic activity and charge transfer efficiency. Excessively thin Au layers may lack sufficient catalytic enhancement, whereas thicker layers are prone to agglomeration, reducing the active surface area and gas adsorption capacity.

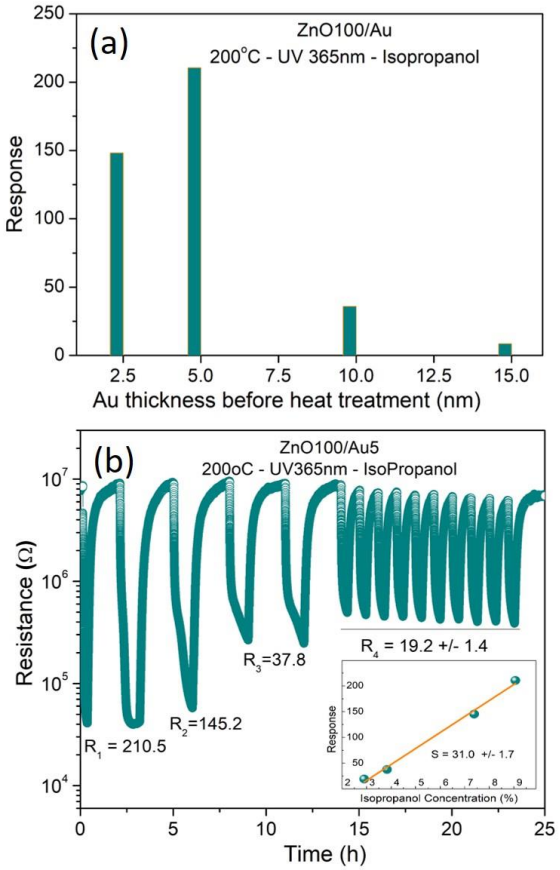

Figure 8. (a) The sensor's response as a function of Au thickness before heat treatment to 9% IPA and (b) the dynamic response of the optimized ZnO100/Au5 sensor to different IPA concentrations at 200 °C under UV 365 nm irradiation. Inset in (b) illustrates a

linear relationship between the sensor response and IPA concentration.

Figure 8(b) demonstrates the dynamic response of the optimized ZnO100/Au5 sensor to different IPA concentrations (9 %, 7.4 %, 3.8 %, and 2.9 %), with corresponding sensor responses of $R_1 \approx 210.5$, $R_2 \approx 145.2$, $R_3 \approx 37.8$, and $R_4 \approx 19.2$, respectively. The results reveal a strong correlation between gas concentration and sensor response, with higher IPA concentrations eliciting stronger responses. The consistent and reversible resistance variations underscore the sensor's stability and reliability for VOC detection. Additionally, the inset graph in Figure 8(b) illustrates a linear relationship between the sensor response and IPA concentration, with a calculated sensitivity of S = 31.0 ± 1.7, highlighting the sensor's potential for accurate VOC quantification. The limit of detection (LOD) can be reasonably estimated by evaluating the standard deviation (δ) and sensitivity (S) from the linear curve fitting of the sensor's response versus gas concentration (%). Using the formula LOD = 3δ/S, with δ = 1.4 and S = 31.0 ± 1.7, the LOD of sensor to IPA is estimated to be approximately 0.136 %. This suggests that the sensor is capable of detecting IPA gas at low concentrations, making it suitable for practical applications.

3.3. Gas sensing mechanism of Au-decorated ZnO under UV365 nm illumination

The gas sensing performance of ZnO-based sensors relies on surface interactions between the target gas molecules and the semiconductor material. When ZnO is exposed to VOCs such as IPA, a series of adsorption, charge transfer, and reaction processes occur at the sensor surface, leading to measurable changes in electrical resistance. However, pristine ZnO often exhibits limitations in selectivity, response magnitude, and operating temperature, necessitating material modifications to enhance its sensing properties.

To address these challenges, Au NPs and UV 365 nm illumination are employed to improve sensor performance through Schottky barrier formation, catalytic effect (spillover), and localized surface plasmon resonance (LSPR) enhancement. The Au NPs act as electron traps, facilitating charge transfer and promoting gas-surface interactions, while UV illumination generates additional charge carriers, accelerating adsorption-desorption dynamics. These synergistic effects lead to an enhanced response, improved selectivity, and reduced operating temperature compared to conventional ZnO sensors.

The gas sensing behavior of ZnO/Au under UV 365 nm illumination is governed by a series of surface reactions, including UV-induced charge carrier generation, oxygen species formation, IPA oxidation, and sensor recovery dynamics. These processes play a crucial role in modulating the sensor's electrical resistance, enabling sensitive and selective IPA detection. The detailed mechanistic steps are outlined below:

Step 1: *Role of Gold Nanoparticles (AuNPs)*

Au NPs function as electron traps, extracting electrons from ZnO and inhibiting their recombination with holes. This process results in the formation of a Schottky barrier at the Au-ZnO interface due to the work function difference ($\Phi_{Au} \approx 5.1$ eV, $\Phi_{ZnO} \approx 4.2$ eV),[26] which induces electron depletion in the ZnO region near the junction. Consequently, this barrier enhances charge separation, extends electron lifetime, and strengthens gas interactions by facilitating more efficient electron transfer during gas adsorption and reaction processes:

$$Au_{nano} + e^- \rightarrow Au^-$$

Step 2: *UV Excitation and Charge Generation*

When ZnO absorbs UV 365 nm light, electrons in the VB gain energy and transition to the CB, creating electron-hole (e_p^- - h_p^+) pairs:[15]

$$ZnO + h\nu(365nm) \rightarrow e_p^- + h_p^+$$

The photogenerated electrons (e_p^-) play a crucial role in modulating gas adsorption and reaction dynamics on the sensor surface.

Step 3: *Oxygen Adsorption and Formation of Reactive Oxygen Species*

In ambient air, oxygen molecules (O_2) adsorb onto the ZnO/Au surface and capture free or/and photogenerated electrons, forming reactive oxygen species that act as active sites for gas sensing:[4,27]

$$O_2(gas) + e^-(or/and\ e_p^-) \rightarrow O_2^-(ads)$$

$$O_2^- + e^-(or/and\ e_p^-) \rightarrow 2O^-$$

These oxygen species are highly reactive and play a key role in oxidizing IPA molecules upon exposure.

Step 4: *Gas Interaction (IPA Oxidation) and Sensor Response*

When IPA molecules interact with O^- species on the sensor surface, they undergo oxidation, releasing electrons back into the ZnO conduction band. This electron injection reduces the sensor's electrical resistance, leading to a strong sensing response:

$$C_3H_8O(IPA) + O^- \rightarrow CO_2 + H_2O + e^-$$

The magnitude of this resistance change is directly correlated with the concentration of IPA molecules, making ZnO/Au an effective IPA sensor.

Step 5: *Sensor Recovery after Gas Removal*

Once the IPA vapor is removed, fresh oxygen molecules from air re-adsorb onto the ZnO/Au surface, restoring the baseline resistance of the sensor:

$$O_2(gas) + e^-(or\ /\ and\ e_p^-) \rightarrow O_2^-(ads)$$

Under UV 365 nm irradiation, this desorption process is significantly accelerated, leading to faster recovery times and ensuring sensor stability over multiple detection cycles.

By leveraging UV-assisted charge carrier generation, Schottky barrier formation at Au-ZnO interfaces, and catalytic oxidation processes, the ZnO/Au sensor achieves high response and efficient recovery for IPA detection.

The size of Au NPs plays a critical role in determining the gas sensing performance of ZnO/Au hybrid sensors, particularly for IPA detection under UV 365 nm irradiation at 200 °C. If the Au NPs are small (ZnO100/Au2.5), they lack the ability to form well-defined Schottky barriers, resulting in weak electron trapping and lower sensor response. Conversely, larger Au NPs (ZnO100/Au10 and ZnO100/Au15) tend to agglomerate, reducing the density of Schottky junctions and limiting their impact on charge modulation. At an optimal size (ZnO100/Au5), Au NPs effectively trap and release electrons, maximizing the gas-induced resistance change and ensuring a strong, reversible sensor response.

In addition to Schottky barrier effects, LSPR enhancement further improves sensor performance. Under UV 365 nm irradiation, Au NPs exhibit plasmonic resonance, generating hot electrons that can be injected into ZnO's conduction band. This process increases free charge carrier concentration, suppresses recombination, and amplifies surface reactions. Smaller Au NPs exhibit weak plasmonic effects, whereas larger particles show broadened and less intense plasmonic peaks, reducing their effectiveness. For ZnO100/Au5, Au NPs exhibit strong LSPR effects, enhancing light absorption, accelerating electron-hole separation, and improving gas adsorption/desorption kinetics.

To gain deeper insight into the sensing mechanism of ZnO/Au structure - particularly under UV irradiation and in the presence of isopropanol (IPA) gas - we propose a model illustrating the energy band alignment and surface adsorption processes under various environmental conditions. These processes are illustrated in detail in Figure 9, which shows the corresponding energy band diagrams (top) and surface adsorption models (bottom) under each condition, highlighting the role of Au nanoparticles in enhancing oxygen adsorption and modulating the sensor response (Figure 9).

Before contact, the difference in work functions between Au and ZnO leads to a misalignment in their Fermi levels (Figure 9a), which drives the formation of a Schottky junction upon contact (Figure 9b). Under dark conditions in air, charge redistribution occurs at the ZnO/Au interface, resulting in upward band bending in ZnO and the formation of a surface electron depletion layer. Additionally, Au nanoparticles facilitate the *spillover* effect, enhancing the adsorption of oxygen species on the ZnO surface (Figure 9b). Upon exposure to UV 365 nm, photogenerated electron–hole pairs further promote the formation of reactive oxygen species and narrowing the depletion region and decreasing the baseline resistance of the sensor (Figure 9c). When IPA gas is introduced, the reducing molecules react with the adsorbed oxygen species, releasing trapped electrons back into the ZnO conduction band. This reaction narrows the depletion layer and decreases the resistance, which serves as the basis for gas detection (Figure 9d).

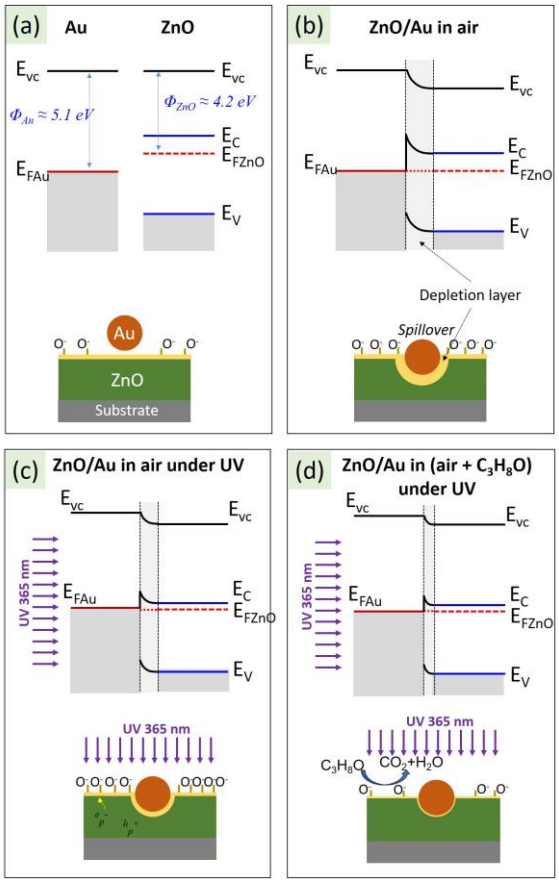

Figure 9. (a) Schematic energy band diagrams (top) and corresponding adsorption models (bottom) illustrating the interfacial and surface processes in the ZnO/Au system under various environmental and optical conditions: (a) Isolated Au and ZnO before contact, where the difference in work function Φ_{Au}, Φ_{ZnO} results in distinct Fermi levels (E_{FAu} and E_{FZnO}); (b) ZnO/Au heterostructure in air under dark condition. Upon contact, electrons transfer from ZnO to Au until Fermi level equilibrium is achieved, leading to the upward band bending in ZnO and the formation of a depletion region near the interface. The presence of Au nanoparticles also facilitates the *spillover* effect, enhancing the adsorption of oxygen species on the ZnO surface; (c) ZnO/Au structure in air under UV (365 nm) illumination. UV excitation generates electron-hole pairs, where photogenerated holes (h^+) participate in the formation of additional surface oxygen species, further narrowing the depletion layer and decreasing the sensor's baseline resistance; (d) ZnO/Au structure in a mixed atmosphere of air and isopropanol (C_3H_8O) under UV illumination. Adsorbed oxygen species react with IPA, producing CO_2 and H_2O and releasing trapped electrons back into the conduction band of ZnO. This reduces the width of the depletion region and leads to a measurable decrease in resistance, which serves as the sensing signal. The energy levels E_{VC}, E_C, E_V, E_{FAu}, and E_{FZnO} represent the vacuum level, conduction band minimum, valence band maximum, Fermi level of Au, and Fermi level of ZnO, respectively.

4. CONCLUSION

This study demonstrates the successful development of ZnO/Au nanostructured sensors for highly sensitive and selective IPA detection under UV365 nm irradiation at 200 °C. The optimized ZnO100/Au5 sensor exhibits outstanding gas sensing properties, with a response of 210.5 to 9 % IPA, a high sensitivity of 31.0 ± 1.7 (1/%), and a low detection limit (LOD) of 0.136% IPA. The superior performance is attributed to the synergistic effects of Au-induced Schottky barrier modulation, plasmonic enhancement, and UV-assisted charge carrier generation, leading to improved adsorption-desorption kinetics and accelerated sensor recovery. Furthermore, the low operating temperature (200 °C) compared to conventional ZnO-based sensors (300 – 400 °C) makes this system more energy-efficient and practical for real-world applications. Although 200 °C is not room temperature, it is still considered a relatively low operating temperature for metal oxide semiconductor gas sensors, particularly those based on ZnO. In many conventional systems, ZnO requires elevated temperatures in the range of 300 – 450 °C to achieve sufficient sensitivity to volatile organic compounds (VOCs) due to the need for thermal activation of surface reactions.[28] The ability of our ZnO-based sensor to exhibit a stable and enhanced response to isopropanol and toluene vapors at 200 °C demonstrates a significant improvement in reducing the thermal budget for sensor operation. Moreover, the application of UV irradiation further enhances sensor response and provides a promising direction for developing gas sensors capable of room-temperature operation in future designs. From an application standpoint, an operating temperature of 200 °C remains acceptable for a wide range of industrial and environmental monitoring systems, where heating elements are integrated and energy consumption is managed efficiently.[29] These findings suggest that our sensor structure has both scientific value and practical potential in real-world conditions.

Given these promising results, ZnO/Au hybrid sensors hold significant potential for real-time VOCs monitoring in various industries, including environmental air quality control, workplace safety, and smart sensor networks for industrial emissions monitoring. The ability to achieve high selectivity and sensitivity at relatively low temperatures positions these sensors as viable candidates for integration into portable and wearable gas detection devices.

However, a notable limitation of the current sensor is its relatively long response and recovery times, which may affect its real-time detection capability in dynamic environments. This delay in sensor reaction could be attributed to slow desorption kinetics of IPA molecules on the ZnO/Au surface, even under UV irradiation. To address this challenge, future studies should focus on optimizing surface functionalization, tuning Au nanoparticle morphology, and exploring alternative catalytic materials to accelerate the gas adsorption-desorption process. Additionally, modifying ZnO with advanced nanostructured materials such as metal-organic frameworks (MOFs), 2D materials (graphene, MXenes), or heterostructures with p-type oxides could further enhance sensor performance by reducing response/recovery times while maintaining high sensitivity and selectivity.

For future research, several directions could further enhance the applicability of this sensor platform. First, optimizing the morphology and surface functionalization of ZnO/Au nanostructures could improve selectivity toward specific VOCs, such as toluene, acetone, and formaldehyde, which are critical pollutants in indoor air quality assessment. Second, integrating ZnO/Au sensors with flexible substrates and wireless communication modules could pave the way for next-generation IoT-based VOC sensing platforms. Third, exploring alternative noble metal catalysts (e.g., Pt, Pd, Ag) and multi-metallic hybrid nanostructures could provide further enhancements in sensor stability, lower detection limits, and multi-gas sensing capabilities.

Overall, this work provides a strong foundation for the design and application of advanced ZnO/Au-based gas sensors, offering a scalable, energy-efficient, and highly responsive solution for VOC detection. With continued optimization and material innovation, these sensors could play a crucial role in future smart sensing technologies for environmental and industrial applications.

REFERENCES

1. R. Montero-Montoya, R. López-Vargas, and O. Arellano-Aguilar. Volatile Organic Compounds in Air: Sources, Distribution, Exposure and Associated Illnesses in Children. *Journal*, **2018**, *84*, 225-238.
2. J. R. W. Kapp, C. Bevan, T. H. Gardiner, M. I. Banton, T. R. Tyler, and G. A. Wright. Isopropanol: Summary of TSCA Test Rule Studies and Relevance to Hazard Identification. *Regulatory Toxicology and Pharmacology*, **1996**, *23*, 183-192.
3. M. Waqas Alam, A. Sharma, A. Sharma, S. Kumar, P. Mohammad Junaid, and M. Awad. VOC Detection with Zinc Oxide Gas Sensors: A Review of Fabrication, Performance, and Emerging Applications. *Electroanalysis*, **2025**, *37*, e202400246.
4. C. Wang, L. Yin, L. Zhang, D. Xiang, and R. Gao. Metal Oxide Gas Sensors: Sensitivity and Influencing Factors. *Journal*, **2010**, *10*, 2088-2106.
5. Y. Shimizu and M. Egashira. Basic Aspects and Challenges of Semiconductor Gas Sensors. *MRS Bulletin*, **1999**, *24*, 18-24.
6. A. Mirzaei, S. G. Leonardi, and G. Neri. Detection of hazardous volatile organic compounds (VOCs) by metal oxide nanostructures-based gas sensors: A review. *Ceramics International*, **2016**, *42*, 15119-15141.
7. R. Kumar, O. Al-Dossary, G. Kumar, and A. Umar. Zinc Oxide Nanostructures for NO2 Gas–Sensor Applications: A Review. *Nano-Micro Letters*, **2015**, *7*, 97-120.
8. M. A. Franco, P. P. Conti, R. S. Andre, and D. S. Correa. A review on chemiresistive ZnO gas sensors. *Sensors and Actuators Reports*, **2022**, *4*, 100100.
9. L.-Y. Zhu, L.-X. Ou, L.-W. Mao, X.-Y. Wu, Y.-P. Liu, and H.-L. Lu. Advances in Noble Metal-Decorated Metal Oxide Nanomaterials for Chemiresistive Gas Sensors: Overview. *Nano-Micro Letters*, **2023**, *15*, 89.

10. S. Kumar, A. Betal, A. Kumar, A. G. Chakkar, P. Kumar, M. Kwoka, S. Sahu, and M. Kumar. Enhancing NO2 Gas Sensing: The Dual Impact of UV and Thermal Activation on Vertically Aligned Nb-MoS2 for Superior Response and Selectivity. *ACS Sensors*, **2025**,
11. N. S. Ramgir, M. Kaur, P. K. Sharma, N. Datta, S. Kailasaganapathi, S. Bhattacharya, A. K. Debnath, D. K. Aswal, and S. K. Gupta. Ethanol sensing properties of pure and Au modified ZnO nanowires. *Sensors and Actuators B: Chemical*, **2013**, *187*, 313-318.
12. J. Hwang, S.-H. Park, Y.-S. Shim, S. Sohn, J. H. Chung, Y.-H. Cho, J. Lee, M. Choi, G. H. Lee, D. Cho, K. Lee, and W. Lee. Fast and selective isoprene gas sensor: Influence of polystyrene size and role of the au catalyst on gas sensing properties. *Sensors and Actuators B: Chemical*, **2025**, *422*, 136500.
13. B. Somalapura Prakasha, G. Shukla, and A. Subramanian. Discriminative analysis of volatile organic compounds using machine-learning assisted Au loaded ZnO and TiO2-based thin film sensors. *Sensors and Actuators A: Physical*, **2024**, *373*, 115385.
14. V. S. Bhati, M. Hojamberdiev, and M. Kumar. Enhanced sensing performance of ZnO nanostructures-based gas sensors: A review. *Energy Reports*, **2020**, *6*, 46-62.
15. F. Xu and H.-P. Ho. Light-Activated Metal Oxide Gas Sensors: A Review. *Journal*, **2017**, *8*,
16. L. D. Bastatas, P. Wagle, E. Echeverria, A. J. Austin, and D. N. McIlroy. The Effect of UV Illumination on the Room Temperature Detection of Vaporized Ammonium Nitrate by a ZnO Coated Nanospring-Based Sensor. *Journal*, **2019**, *12*,
17. J. Gong, Y. Li, X. Chai, Z. Hu, and Y. Deng. UV-Light-Activated ZnO Fibers for Organic Gas Sensing at Room Temperature. *The Journal of Physical Chemistry C*, **2010**, *114*, 1293-1298.
18. M. S. Rodrigues, J. Borges, C. Lopes, R. M. S. Pereira, M. I. Vasilevskiy, and F. Vaz. Gas Sensors Based on Localized Surface Plasmon Resonances: Synthesis of Oxide Films with Embedded Metal Nanoparticles, Theory and Simulation, and Sensitivity Enhancement Strategies. *Journal*, **2021**, *11*,
19. G. Wang, P. Wu, L. Guo, W. Wang, W. Liu, Y. Wang, T. Chen, H. Wang, Y. Xu, and Y. Yang. Preparation of Au@ZnO Nanofilms by Combining Magnetron Sputtering and Post-Annealing for Selective Detection of Isopropanol. *Journal*, **2022**, *10*,
20. S. K. Arya, S. Saha, J. E. Ramirez-Vick, V. Gupta, S. Bhansali, and S. P. Singh. Recent advances in ZnO nanostructures and thin films for biosensor applications: review. *Anal Chim Acta*, **2012**, *737*, 1-21.
21. R. Yan, T. Takahashi, H. Zeng, T. Hosomi, M. Kanai, G. Zhang, K. Nagashima, and T. Yanagida. Robust and Electrically Conductive ZnO Thin Films and Nanostructures: Their Applications in Thermally and Chemically Harsh Environments. *ACS Applied Electronic Materials*, **2021**, *3*, 2925-2940.
22. N. M. Vuong, T. T. Hien, V. T. Han, H. N. Hieu, and N. Van Nghia. Efficient performance acetone sensor based on squirrel-tail like Ni doped ZnO hierarchical nanostructure. *Materials Characterization*, **2021**, *180*, 111388.
23. N. M. Vuong, D. D. Duy, H. N. Hieu, V. N. Nguyen, N. N. K. Truong, H. Van Bui, and N. Van Hieu. Low-operating temperature and remarkably responsive methanol sensors using Pt-decorated hierarchical ZnO structure. *Nanotechnology*, **2022**, *33*, 065502.
24. S. Park, S. An, Y. Mun, and C. Lee. UV-Enhanced NO2 Gas Sensing Properties of SnO2-Core/ZnO-Shell Nanowires at Room Temperature. *ACS Applied Materials & Interfaces*, **2013**, *5*, 4285-4292.
25. H. Ji, W. Zeng, and Y. Li. Gas sensing mechanisms of metal oxide semiconductors: a focus review. *Nanoscale*, **2019**, *11*, 22664-22684.
26. J. Kim, J.-H. Yun, C. H. Kim, Y. C. Park, J. Y. Woo, J. Park, J.-H. Lee, J. Yi, and C.-S. Han. ZnO nanowire-embedded Schottky diode for effective UV detection by the barrier reduction effect. *Nanotechnology*, **2010**, *21*, 115205.
27. A. Gurlo. Interplay between O2 and SnO2: Oxygen Ionosorption and Spectroscopic Evidence for Adsorbed Oxygen. *ChemPhysChem*, **2006**, *7*, 2041-2052.
28. G. Korotcenkov. Metal oxides for solid-state gas sensors: What determines our choice? *Materials Science and Engineering: B*, **2007**, *139*, 1-23.
29. J.-H. Lee. Gas sensors using hierarchical and hollow oxide nanostructures: Overview. *Sensors and Actuators B: Chemical*, **2009**, *140*, 319-336.